Acta Biomaterialia 111 (2020) 290–301

Contents lists available at ScienceDirect

Acta Biomaterialia

journal homepage: www.elsevier.com/locate/actbio

Full length article

Structure and composition of the tunic in the sea pineapple *Halocynthia roretzi*: A complex cellulosic composite biomaterial

Geonho Song[a,1], Jérôme Delroisse[b,1], Dorian Schoenaers[b], Hyungbin Kim[c], Thai Cuong Nguyen[d], Nils Horbelt[a], Philippe Leclère[d], Dong Soo Hwang[c,*], Matthew J. Harrington[a,e,**], Patrick Flammang[b,*]

[a] Department of Biomaterials, Max Planck Institute of Colloids and Interfaces, Research Campus Golm, 14424 Potsdam, Germany
[b] Biology of Marine Organisms and Biomimetics Unit, Research Institute for Biosciences, University of Mons, 23 Place du Parc, 7000 Mons, Belgium
[c] Division of Environmental Science and Engineering, Pohang University of Science and Technology (POSTECH), Pohang 37673
[d] Laboratory for Chemistry of Novel Materials, Center for Innovation and Research in Materials and Polymers (CIRMAP), University of Mons, 23 Place du Parc, 7000 Mons, Belgium
[e] Department of Chemistry, McGill University, 801 Sherbrooke Street West, Montreal, Quebec H3A 0B8, Canada

ARTICLE INFO

Article history:
Received 3 January 2020
Revised 20 April 2020
Accepted 21 April 2020
Available online 11 May 2020

Keywords:
Tunicata
Ascidiacea
Cellulose-based material
Dityrosine cross-links
Bromotyrosine
Helicoidal structure

ABSTRACT

Biological organisms produce high-performance composite materials, such as bone, wood and insect cuticle, which provide inspiration for the design of novel materials. Ascidians (sea squirts) produce an organic exoskeleton, known as a tunic, which has been studied quite extensively in several species. However, currently, there are still gaps in our knowledge about the detailed structure and composition of this cellulosic biocomposite. Here, we investigate the composition and hierarchical structure of the tough tunic from the species *Halocynthia roretzi*, through a cross-disciplinary approach combining traditional histology, immunohistochemistry, vibrational spectroscopy, X-ray diffraction, and atomic force and electron microscopies. The picture emerging is that the tunic of *H. roretzi* is a hierarchically-structured composite of cellulose and proteins with several compositionally and structurally distinct zones. At the surface is a thin sclerotized cuticular layer with elevated composition of protein containing halogenated amino acids and cross-linked via dityrosine linkages. The fibrous layer makes up the bulk of the tunic and is comprised primarily of helicoidally-ordered crystalline cellulose fibres with a lower protein content. The subcuticular zone directly beneath the surface contains much less organized cellulose fibres. Given current efforts to utilize biorenewable cellulose sources for the sustainable production of bio-inspired composites, these insights establish the tunic of *H. roretzi* as an exciting new archetype for extracting relevant design principles.

Statement of Significance

Tunicates are the only animals able to produce cellulose. They use this structural polysaccharide to build an exoskeleton called a tunic. Here, we investigate the composition and hierarchical structure of the tough tunic from the sea pineapple *Halocynthia roretzi* through a multiscale cross-disciplinary approach. The tunic of this species is a composite of cellulose and proteins with two distinct layers. At the surface is a thin sclerotized cuticular layer with a higher protein content containing halogenated amino acids and cross-linked via dityrosine linkages. The fibrous layer makes up the bulk of the tunic and is comprised of well-ordered cellulose fibres with a lower protein content. Given current efforts to utilize cellulose to

* Corresponding authors.
** Corresponding author at: Department of Chemistry, McGill University, 801 Sherbrooke Street West, Montreal, Quebec H3A 0B8, Canada.
E-mail addresses: dshwang@postech.ac.kr (D.S. Hwang), matt.harrington@mcgill.ca (M.J. Harrington), Patrick.Flammang@umons.ac.be (P. Flammang).
[1] These authors contributed equally to this work.

https://doi.org/10.1016/j.actbio.2020.04.038

produce advanced materials, the tunic of the sea pineapple provides a striking model for the design of bio-inspired cellulosic composites.

1. Introduction

Ascidians, commonly known as sea squirts or tunicates, are sac-like, filter-feeding, sessile marine invertebrates belonging to the subphylum Tunicata which is part of the chordate group [1,2]. As the name of the subphylum implies, these organisms are encased in a characteristic, primarily organic exoskeleton called a tunic. Depending on the species, this tunic comes in an astonishing array of colours and in every shade, from pure white to jet black [3]. Its consistency also varies enormously, from soft and gelatinous to tough and leathery [3,4]. The tunic has a number of roles including a supportive function, maintaining the animal's shape and preventing the collapse of its internal cavities, and a protective function, isolating the animal from the external environment and from invasive microorganisms, foulers, and predators [3,5]. The tunic also anchors the animal to the substrate. The tunic always comprises two layers, a thin and dense outer layer and a broad, loosely structured inner layer bordering the epidermal cells, and its thickness can reach 8–10 mm in solitary ascidians [4,5]. Like most invertebrate cuticles, the tunic is composed of varying amounts of proteins, carbohydrates, and water, but it also has several features that are unique to ascidians [4,5]. One is the presence of large amounts of structural fibres composed of cellulose [6]. Tunicates are the only animals that produce cellulose and they presumably acquired this ability through a horizontal transfer of a bacterial cellulose synthase gene into the tunicate lineage [7–9]. Another unique feature is the presence of free cells in the tunic, making the tunic a mesenchyme-like tissue [10]. The tunic is secreted in part by the cells it contains and in part by the epidermis of the body wall [3,10].

Sea squirts of the genus *Halocynthia* belong to the family Pyuridae which comprises solitary ascidians characterized by a thick and tough tunic [3,11]. The morphology and composition of the tunic have been studied quite extensively in different species of this genus, such as *H. aurantium* [12,13], *H. papillosa* (e.g., [14,15]), and *H. roretzi* [16,17]. In these species, the tunic is orange to red in colour and its thickness ranges from 1 mm in *H. papillosa* to 2.3 mm in *H. roretzi*. As in other ascidian species, the tunic in *Halocynthia* consists of a thin, dense outer layer, improperly called cuticle (in fact, it is the whole tunic which corresponds to the definition of a cuticle; [18]), and a thick fibrous inner layer named matrix, fundamental substance or tunic main body [12,14,16]. In *H. aurantium* and *H. papillosa*, the cuticular layer, about 50 µm in thickness, is made up of numerous plates, each bearing one or two spines [12,14]. In *H. roretzi*, this layer is variable in thickness [16]. The thick matrix layer is made up of stacked fibrous laminae whose constitutive fibres run parallel to the tunic surface [12,14,16]. Histochemistry revealed that the cuticular layer stains mostly for proteins (sometimes described as scleroproteins) while the fibrous layer stains strongly for acidic mucopolysaccharides and weakly for proteins [13,14]. More detailed biochemical analyses revealed that the fibres of the fibrous inner layer of the tunic consist of a core made up of cellulose sheathed in a material consisting of acid mucopolysaccharides and proteins [15,19]. These studies also revealed that these fibres are also present in the cuticular layer, although in a lower proportion, where they are embedded in a matrix of proteins rich in cysteine [15,19,20]. Whereas the tunic cellulose is synthesized by the epidermal cells [7,21], the associated proteins appear to be produced by specific tunic cells such as granular cells for the fibre-associated proteins and globular cells for the cuticular proteins [16,20,22].

Currently, there is an increasing interest in materials with excellent mechanical properties combined with economical production, while still being sustainable. Because of its availability and properties, as well as renewability, cellulose is considered an important resource for the development of such advanced materials [23]. Cellulose-based structures, such as nanofibrils and nanocrystals, are usually assembled with other (bio)polymers to form fibres, films, or bulk materials which may find applications in diverse industrial sectors [23,24]. Generally, cellulose for biomaterial production is obtained from plant materials or bacterial biomass; however, tunic cellulose is becoming increasingly used and *H. roretzi* is one of the species commonly used for cellulose extraction [25]. This edible species is found in the waters surrounding Korea and Japan where it is also cultivated commercially for the seafood market [26]. Individuals of *H. roretzi* possess an ovoid body covered with large conical bumps (Fig. 1(a)). Apically, the body presents two siphons used as water inlet and outlet for filter-feeding while, basally, it bears many branching roots used in attachment to rocks (Fig. 1(a)). Most parts of the tunic have an orange or red colour except the roots which are dark green to brown.

Understanding how this species uses cellulose to build its tough tunic may provide new insights to inspire the ongoing development of sustainable cellulosic composite materials from biorenewable sources for applications in the biomedical or wastewater treatment fields, for example [25,27,28]. As an animal source, as opposed to plants, the tunic of *H. roretzi* may offer unique insights into material design, especially considering that tunicate cellulose microfibrils are thicker and have a higher aspect ratio compared to those of plants, and that tunicates do not contain hemicelluloses as a matrix material but appear to use proteins instead [25,29]. Although there are many reports on the ascidian tunic, its exact structure and composition are still not fully understood. The primary aim of this investigation is to analyse the tunic in the species *H. roretzi* through a cross-disciplinary approach combining traditional histology, immunohistochemistry, vibrational spectroscopy, X-ray diffraction, and atomic force and electron microscopies, in order to extract an integrated understanding of (a) what biomolecules the tunic is comprised of and (b) how the biomolecules are organized within the different parts of the tunic. Thus, this study of the tunic of *H. roretzi* is expected to provide valuable knowledge especially for the field of material science based on biopolymers.

2. Materials and methods

2.1. Collection of animals and tunic sample preparation

Individuals of *Halocynthia roretzi* (Drasche, 1884) were obtained from the fish market in Pohang city (Gyeongsangnam-do, South Korea). The average size of these aqua-farmed (~2-year old) tunicates is 11 cm × 7 cm (body height and width, respectively). A total of 10 sea squirts were used for this study. After dissection and removal of all the internal organs, the tunic was either stored in 70% ethanol at 4 °C or cut into pieces that were fixed by immersion in 4% solutions of paraformaldehyde or glutaraldehyde in MilliQ water. Only tunic samples taken at mid-height of the body (i.e., excluding the apical siphons and the basal

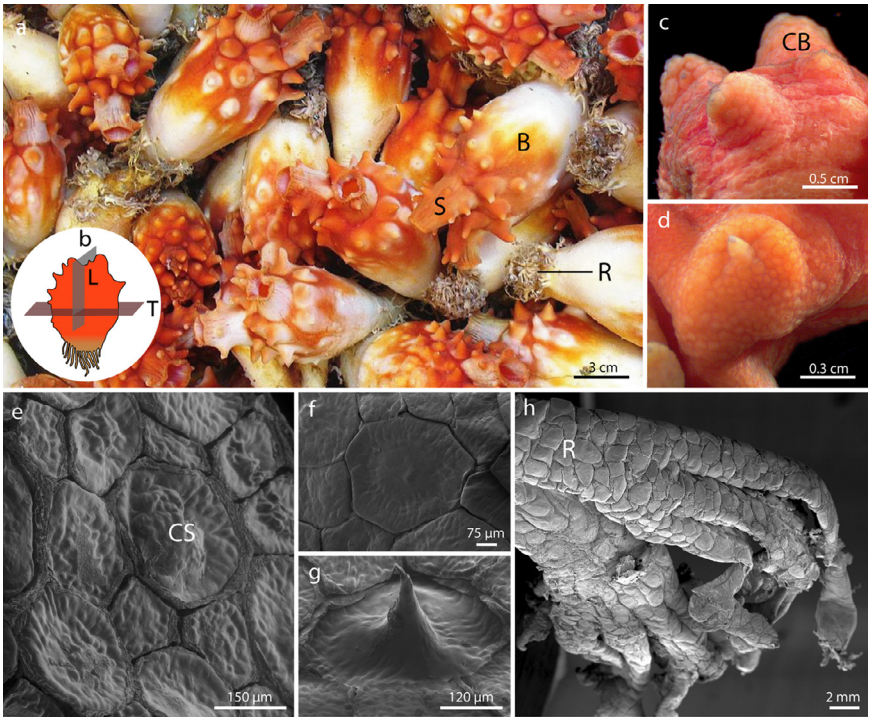

Fig. 1. External morphology of *Halocynthia roretzi* and outer aspect of the tunic. (a) Several individuals in a tank after collection. (b) Schematic drawing of a sea squirt showing the orientation of the sections made for the different experiments. (c,d) Close-up pictures of the conical bumps at the level of the body. (e–g) SEM micrographs of the cuticular scales covering the whole body. (h) Detail of the roots (SEM) showing the progressive reduction of the scales towards their tip. Abbreviations: B, body; CB, conical bump; CS, cuticular scale; L, longitudinal; R, roots; S, syphon; T, transverse. (For interpretation of the references to colour in this figure, the reader is referred to the web version of this article.)

roots) were used in this study (Fig. 1(b)). For many measurements, thin sections were cut for analysis, including histological investigation, FTIR spectroscopy, Raman spectroscopy and WAXD analysis. In most cases, longitudinal and transverse sections were utilized as illustrated in Fig. 1(b).

Animals used in this study were treated in compliance with institutional ethical use protocols.

2.2. Histology, histochemistry and immunohistochemistry

Unstained native sections (10 µm in thickness) obtained by vibratome from ethanol-fixed tunic samples and collected on polylysine-coated glass slides were used for polarized light microscopy (PLM). A Leica DM RXA 2 light microscope system with two polarization filters was employed and images were acquired with a Leica DFC480 digital camera after adjusting saturation, gain, and exposure. PLM measurements were performed on a total of 19 longitudinal sections acquired from at least 6 individuals with similar results for all samples.

Paraformaldehyde-fixed tunic pieces were dehydrated in a sequence of graded ethanol and embedded in paraffin wax (Paraplast, Sigma) using a routine method. Longitudinal and transverse sections (7 µm in thickness) were cut with a Microm HM 340E microtome and collected on clean glass slides. They were stained with Heidenhain's azan trichrome and Masson's trichrome [30]. Some unstained sections were also observed in epifluorescence microscopy. Histochemical observations were performed using the periodic acid-Schiff (PAS) and Astra blue techniques for the detection of polysaccharides, and the alcian blue staining at pH 1 and 2.5 for the detection of polyanionic macromolecules [30]. The presence of DOPA (3,4-dihydroxyphenylalanine) or TOPA (trihydroxyphenylalanine) in the tunic was investigated by using the nitro blue tetrazolium (NBT) redox cycling method [31] and Arnow's staining [32]. All sections were observed with a Zeiss Axioscope A1 microscope equipped with an AxioCam 305 digital camera (Carl Zeiss MicroImaging). For autofluorescence detection, the following filter sets were used: Zeiss Filter Sets 44 (excitation BP 475/40, beamsplitter FT 500, emission BP 530/50), 45 (excitation BP 560/40, beamsplitter FT 585, emission BP 630/75), and 49 (excitation G 365, beamsplitter FT 395, emission BP 445/50).

For immunohistochemistry, paraffin sections were subjected to an indirect immunofluorescence staining method according to the following protocol. After antigen demasking by microwaving sections in citrate buffer (10 mM, pH 6.0), non-specific background staining was blocked by section pre-incubation in phosphate-buffered saline containing 3% bovine serum albumin (Sigma) (PBS-BSA). Monoclonal anti-bromotyrosine antibodies (clone BTK-94C; Santa Cruz Biotechnology, ref. sc-293152), diluted 1:100 in PBS-BSA, were then applied for 1 h at room temperature. After several washes in PBS, the sections were incubated for 1 h in Alexa Fluor 568-conjugated goat anti-mouse immunoglobulins (Life Technologies) diluted 1:100 in PBS-BSA. Following three final washes in PBS, the sections were mounted in Vectashield (Vector Laboratories). The sections were observed and imaged with the Axioscope A1 microscope.

2.3. Transmission electron microscopy (TEM)

For TEM, glutaraldehyde-fixed tunic pieces were rinsed in cacodylate buffer (0.2 M. pH7.8, with 1.84% NaCl) and then post-fixed in 1% osmium tetroxide in cacodylate buffer (0.1 M. pH7.8, with 2.3% NaCl). After rinsing in cacodylate buffer, they were dehydrated in graded ethanol and embedded in Spurr resin. Ultrathin sections (80 nm) were cut with a Leica Ultracut UCT ultramicrotome equipped with a diamond knife. They were contrasted with uranyl acetate and lead citrate and observed with a Zeiss LEO 906E transmission electron microscope.

2.4. Scanning electron microscopy (SEM) and microanalysis

For secondary electron and backscattered electron imaging of tunic pieces, paraformaldehyde- or ethanol-fixed samples were dehydrated in graded ethanol, dried by the critical-point method, and mounted on aluminium stubs using carbon adhesive tabs. Some samples were then coated with gold in a sputter-coater but others were left uncoated. Images were collected using a JEOL JSM-7200F field emission scanning electron microscope or a FEI Quanta 600F environmental scanning electron microscope.

X-ray microanalysis and elemental mapping were performed on uncoated SEM samples or on thin (10 µm) vibratome sections of the tunic by using an Oxford X-Max^N energy-dispersive spectrometer (EDS) equipped with an 80 mm^2 silicon drift detector. Acquisition conditions on the SEM were 15 kV, 10 mm working distance and 10 s live time acquisition at approximately 30–40% dead time. The spectra were acquired with an AZtec (Oxford Instrument) EDS data processing software.

2.5. Atomic force microscopy (AFM)

Paraffin wax transverse sections (10 µm in thickness) through the tunic were collected on clean microscope glass slides, dewaxed in toluene and stored in MilliQ water. The wet tunic sections were then imaged in air and under ambient conditions with a Dimension Icon (Bruker Nano Inc., Santa Barbara, CA) using AFM in Tapping Mode (TM). In TM-AFM, the tip was driven near the resonant frequency and the interactive force between tip and sample was significantly minimized. By doing this, the morphology of the samples was less affected during the experiment. Silicon tip (NCHV, Bruker Nano Inc) with resonant frequency of approximately 320 kHz and nominal spring constant of 40 N/m were employed. The tip radius was determined by the manufacturer as 10 nm. All the images were recorded with a resolution of 512 pixels/line using the Nanoscope software (Version 9.4). The scan rate was kept at 0.5 Hz. The Tapping height and phase images were analysed using Nanoscope Analysis image processing software (Version 1.90). The images were not filtered and only a 2nd order flattening procedure was applied to the raw data.

2.6. Fourier-transform infrared (FTIR) spectroscopy

The tunic of *H. roretzi* was cut into 10 µm thick sections using a vibratome and prepared on a KBr salt sample window. Spectra of the tunic cuticle were acquired at 25 °C with a Bruker Hyperion FTIR microscope (Hyperion 2000) coupled with a Bruker Tensor spectrometer (Ettlingen, Germany). For each measurement, 32 interferograms were accumulated at a spectral resolution of 4 cm^{-1}. The background was measured from an empty region of the window near the sample position. Absorption and transmission spectra were measured for each position. Data were analysed with the OPUS software from Bruker. Data were acquired from more than 10 different sections (both longitudinal and transverse) acquired from at least 3 individuals with similar results for all samples.

2.7. Raman spectroscopy

Raman spectroscopy was performed on both longitudinal and transverse sections of the tunic cut with a vibratome (10 µm thickness) and prepared on polylysine-coated glass slides. A green laser (Nd:YAG laser, λ = 532 nm) was focused using a Confocal Raman Microscope (Alpha300, Witec, Ulm, Germany) equipped with a piezo scanner (P-500, Physik Instrumente, Karlsruhe, Germany). The scattered light was detected by a thermoelectrically cooled CCD detector (DU401A-BV, Andor, Belfast, North Ireland) placed behind the spectrometer (UHTS 300, WITec, Ulm, Germany). Due to high fluorescence of the cuticular layer using the green laser, a near-infrared laser (λ = 785 nm, Toptica Photonics AG, Graefelfing, Germany) was utilized to acquire spectra from 10 µm thick vibratome sections placed on quartz slides. Spectra were collected using a 20× or a 50× objective (Nikon) either as individual spectra acquired from at least five spectra from different spots inside each layer (integration time of 1 s and 20 accumulations) or as area scans of specific regions of the section with a lateral resolution of 0.5 µm and integration time of 1 s. Data were collected from more than 20 different sections acquired from more than 6 individuals with similar results for all samples. Individual spectra from a single sample were averaged and background corrected. ScanCtrl-SpectroscopyPlus software (version 1.60, Witec) was used for collecting data and the OPUS software (Bruker, Germany) for spectral processing of all Raman data.

2.8. Amino acid analysis

For amino acid analysis, the cuticle was separated from the rest of the tunic using a scalpel blade. Ten mg of dried cuticular material was hydrolysed in 6 N HCl with 5% saturated phenol for 24 h at 110 °C in vacuo. After hydrolysis, the hydrolysates were dried and washed with water and methanol 2 times. Amino acid concentrations were measured on a SYKAM S433 amino acid analyser (SYKAM, Germany).

Peroxidase-catalysed dityrosine formation was used for the synthesis of a dityrosine standard [33]. Briefly, 181 mg (1 mmol) of L-tyrosine (Sigma) was dissolved in 200 ml of 0.2 M sodium borate buffer (pH 9.5). 1.1 ml of 3% hydrogen peroxide solution (Sigma) and 3 mg of horseradish peroxidase (Sigma) were added to the solution and then it was incubated at 37 °C for 24 h. 50 ml of the solution were dried by a using rotary evaporator at 60 °C and the resulting powder was dissolved in 2 ml of 0.1 N HCl and left for 48 h.

2.9. X-ray diffraction (XRD)

Synchrotron wide-angle X-ray diffraction (WAXD) experiments were conducted at the mySpot beamline at the BESSY II synchrotron radiation facility (Helmholtz-Zentrum Berlin, Adlershof). Longitudinal vibratome sections (50 µm in thickness) of the tunic were mounted on a plastic foil attached to an aluminium frame. A continuous line scan was made across the section moving from the cuticle to the inner region of the matrix, using an X-ray beam of 10 µm. The wavelength of the incident beam was 0.082656 nm. WAXD patterns were collected with a 2D CCD detector (Rayonix MAR Mosaic225, USA) with a total area of 3072 × 3072 pixels and a pixel size of 73.2 µm × 73.2 µm at a sample-to-detector distance of ~30 cm. WAXD scans were acquired from 5 different longitudinal sections acquired from several different individuals with similar results.

2.10. Statistical analysis

For all measurements, between 2 and 8 individuals were tested, depending on the method used, with several samples or sections measured for each individual. All data are reported as means ± SD. Further experimental details relevant to the specific techniques are included in the respective results section.

3. Results and discussion

3.1. General organisation and fine structure of the tunic

High magnification images of the outer surface of the tunic reveal that it consists of numerous scale-like structures (Fig. 1(c,d)).

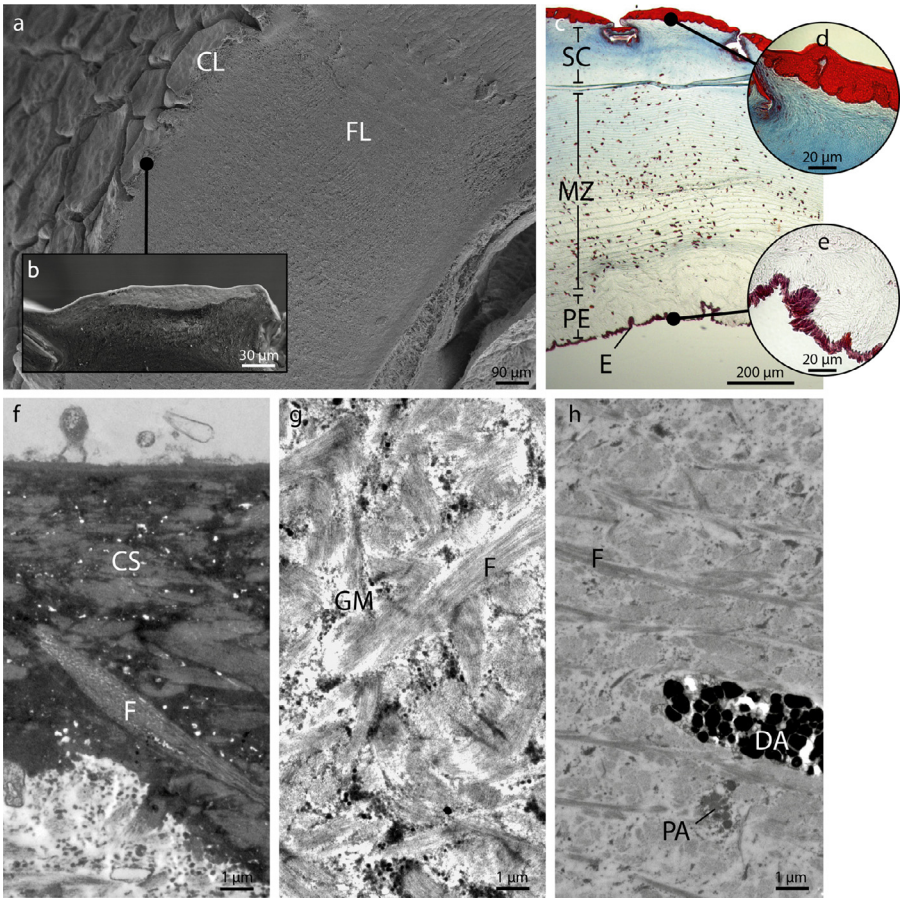

Fig. 2. General organisation and ultrastructure of the tunic of *Halocynthia roretzi*. (a–e) Transverse sections through the tunic observed in SEM (a,b) and in light microscopy after Azan trichrome staining (**c–e**). (b,d) Details of a cuticular scale on top of the subcuticular zone. (e) Detail of the epidermis and the peri-epidermal zone. (f–h) TEM micrographs showing a cuticular scale, the subcuticular zone, and the median zone of the fibrous layer, respectively. Abbreviations: CL, cuticular layer; CS, cuticular scale; DA, dense-granular amoebocyte; E, epidermis; F, fibre; FL, fibrous layer; GM, granular material; MZ, median zone; PA, pale-granular amoebocyte; PE, peri-epidermal zone; SC, subcuticular zone.

These polygonal scales have a wrinkled surface and range from 100 µm up to 1 mm in diameter (Fig. 1(e,f)). They interlock like tiles to completely cover the body. Although most of the scales are flat, a few of them present a pointed, spine-like shape measuring up to 500 µm in height (Fig. 1(g)). This is different from *H. aurantium* and *H. papillosa* in which each scale bears one to several shorter (200–300 µm) spines [12,14]. The roots also bear scales, but they are smaller, smoother, and less conspicuous than on the body. Scales decrease in size towards the tip of the roots where they are no longer visible (Fig. 1(h)).

Transverse sections at mid-body level show that the tunic measures about 1.2 mm in thickness (Fig. 2(a,c)). It is made up of two layers which differ by their aspect and tinctorial affinity: the outer cuticular layer comprising the scales and the inner fibrous layer. The cuticular material appears as dense and compact (Fig. 2(b)). It is brightly stained in red with topographical trichrome stains (Fig. 2(c,d)). In section, each scale presents a semi-lenticular shape with a maximum thickness of about 40 µm. The scales are not independent of each other but are connected by very thin (250–300 nm) cuticular folds. Miniature scales can sometimes be observed within these folds. No cells are visible in the cuticular layer. The fibrous layer, which comprises the bulk of the tunic, consists of three sub-layers: the sub-cuticular zone, the median zone, and the peri-epidermal zone. The term ‘zone’ is used instead of ‘layer’, because the boundaries between zones are difficult to define precisely. The fibrous layer is very weakly stained with topographical trichrome stains. The sub-cuticular zone ranges between 200 and 250 µm in thickness. On sections, it presents a crenelated aspect, each crenel being topped by a cuticular scale (Fig. 2(a,c)). The cells present in this zone are mostly located in the vicinity of the cuticular folds. The median zone is the thickest of the three zones (about 800 µm). It is characterized by a conspicuous layered structure whose layers are more closely packed outward (distance between layers 6.8 ± 1.9 µm, $n = 4$ individuals) than inward (distance between layers 14.4 ± 4.8 µm). This zone is richly populated with cells which are homogeneously distributed. The peri-epidermal zone, lastly, is about 150 µm thick. It is less structured than the median zone (distance between layers 31.8 ± 10.3 µm) and contains fewer cells. The tunic morphology in *H. roretzi* is very similar to what has been described in other species of *Halocynthia* [12,14].

TEM images show that both the cuticular and fibrous layers consist of fibres embedded in a ground substance (Fig. 2(f–h)). These fibres are, in turn, made up of nanofibrils (Fig. 2(g)). As observed in light microscopy, the fibres present in the median zone of the fibrous layer run parallel to the tunic surface and are arranged in a layered structure with a periodicity between sublayers presenting the same fibre orientation ranging from about 3 to 20 µm according to the area observed (Fig. 2(c,h)). In the subcuticular zone, the fibres are more densely packed and their arrangement of seems more random, the micrographs showing a criss-cross of fibres (Fig. 2(g)). In this zone, the matrix around the fibres contains clusters of electron-dense granular material (granules measuring 80–110 nm in diameter) which become more abundant

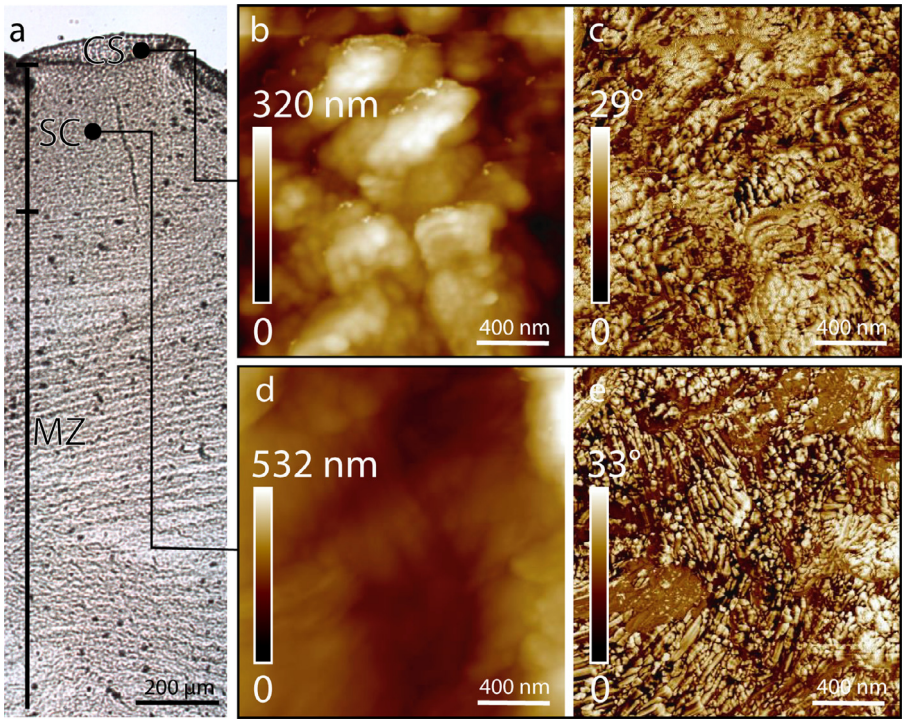

Fig. 3. Tapping-mode atomic force microscopy of sections made through the tunic of *Halocynthia roretzi*. (a) Light microscope image of a transverse tunic section used for TM-AFM analysis, showing scanned areas. Height images (b,d) and corresponding phase images (c,e) of the cuticular layer (b,c) and of the subcuticular zone of the fibrous layer (d,e). Abbreviations: CS, cuticular scale; MZ, median zone; SC, subcuticular zone.

closer to the cuticular layer (Fig. 2(f,g)). Some of the fibres from the subcuticular zone clearly extend into the cuticular layer where they are embedded in a much more electron-dense matrix which seems to originate from the coalescence of the granular material (Fig. 2(f)). This fibre continuity between the subcuticular zone and the cuticular layer was already reported in *H. papillosa* [15], but is observed for the first time in *H. roretzi* in which earlier TEM studies rather described a clear boundary between these two tunic areas [16,17].

TM-AFM observations corroborate the TEM results. In height images, both the cuticular layer and the subcuticular zone of the fibrous layer appear bulgy (Fig. 3(a,c)) and the corresponding phase images suggest each bulge could correspond to an oblique section through a fibre as it contains a bundle of stiffer nanofibrils (Fig. 3(b,d)). These nanofibrils have a diameter of 34.7 ± 6.6 nm (n = 40 nanofibrils). The smallest ones, presumably corresponding to perpendicular cross-sections, measure about 25 nm, which corresponds to the size of the cellulose-protein fibrils described in the genus *Halocynthia* [25,34].

Different types of cells populate the different zones of the tunic fibrous layer (Fig. 2(c,d)). In addition to a few phagocytes (not illustrated), four types of granulocytes were observed, two in the subcuticular zone and two in the median zone, which will be named according to the terminology of Hirose et al. [16]. In the subcuticular zone, cells are located in the vicinity of the cuticular folds and are always surrounded by an abundant electron-dense granular material. These cells comprise globular cells and vacuolated cells. The former are the most abundant and contain spherical secretory granules measuring 485 ± 43 nm (n = 15 granules) in diameter and enclosing electron-dense material surrounded by an electron-lucent rim (Fig. 4(a)). The latter, sparser, are characterized by larger vacuoles (from 1 up to 3 µm in diameter) appearing empty or filled with a very electron-dense material (Fig. 4(b)). In the median zone, the most abundant cells are dense-granular amoebocytes. These cells are packed with polyhedral granules measuring 785 ± 92 nm (n = 10 granules) and filled with a very electron-dense contents showing a striation pattern (Fig. 4(c)). On some images, a fraction or all of these granules appear empty suggesting that their contents have been released. Finally, pale-granular amoebocytes are also occurring in the median zone. These cells contain spherical granules measuring 370 ± 58 nm (n = 10 granules) and enclosing a material of medium electron-density (Fig. 4(d)). Similar cells were described in the fibrous layer of the tunic of *H. aurantium* and *H. papillosa* [12,14,15]. All these cells are assumed to be involved in the synthesis of tunic materials. Indeed, although cellulose is produced by the epidermal cells [7,8,21], the other components of the fibrils and of the matrix are likely produced by tunic granulocytes as evidenced by earlier studies [16,20,22] and by the granular material surrounding some of these cells and which is of similar electron-density to the cell contents.

3.2. Composition of the tunic

The observed differences in the structure of the cuticular and fibrous layers evident in microscopic imaging suggests they are likely comprised of different biomolecular components, as previously suggested [13–15]. Histochemical staining has therefore been used to investigate the tunic gross chemical composition. The whole tunic (i.e. both the cuticular and fibrous layers) is stained with Astra blue, a dye targeting cellulose, but when acid fuschin is used as a counterstain, only the fibrous layer is stained blue while the cuticular layer is stained bright red, indicative of a prominent protein content (Fig. 5(a)). Similarly, with the PAS method which stains neutral polysaccharides and glycoproteins, the whole tunic is stained pink, but the fibrous layer is also lightly stained blue with the luxol blue counterstain which highlights basic proteins (Fig. 5(b–d)). Conversely, alcian blue stains the fibrous layer, both at pH 1 (Fig. 5(e)) and pH 2.5 (not illustrated), but not the cuticular layer (Fig. 5(f)). This dye targets anionic polysaccharides, binding only sulphate groups at pH 1 and both sulphate and carboxylate

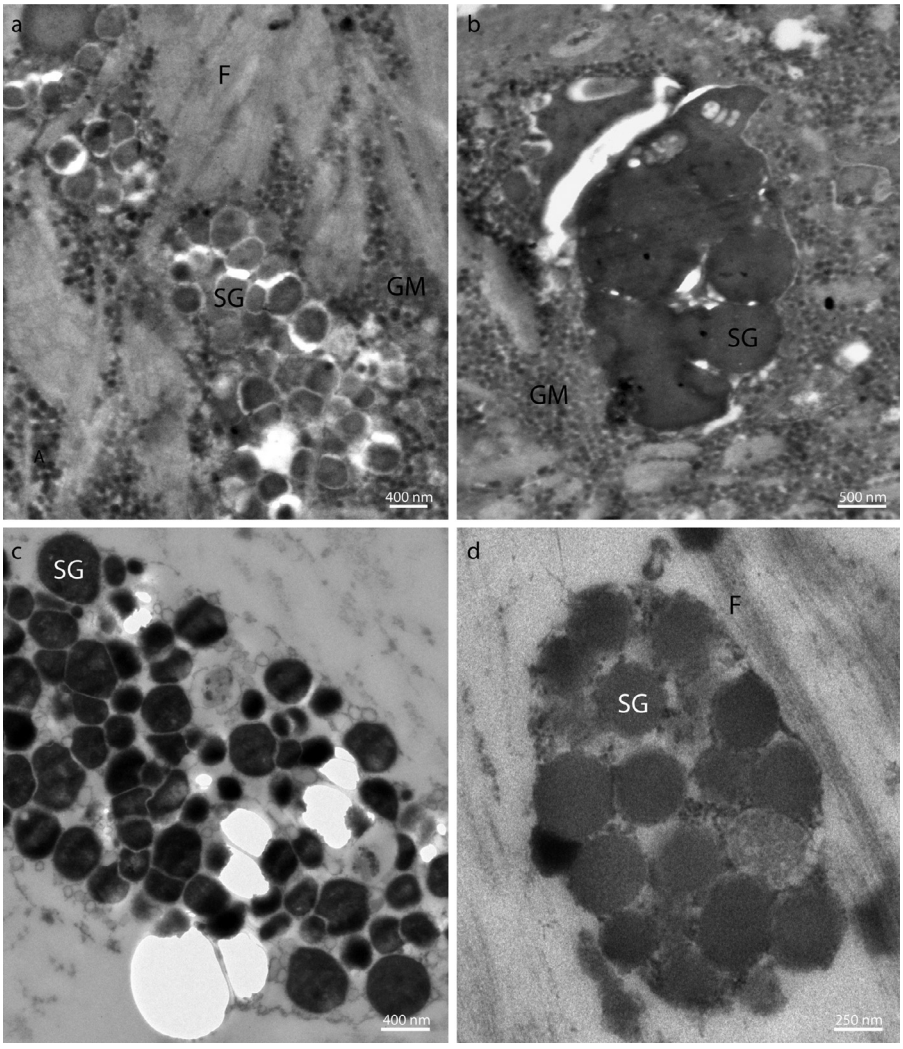

Fig. 4. TEM micrographs of the different types of granulocytes occurring in the tunic of *Halocynthia roretzi*. Globular cells (a) and vacuolated cells (b) are observed within the subcuticular zone, close to the cuticular folds. Dense-granular amoebocytes (c) and pale-granular amoebocytes (d) occur in the median zone of the fibrous layer. Abbreviations: F, fibre; GM, granular material.

groups at pH 2.5. With these different methods, a staining gradient can be observed in the fibrous layer, the sub-cuticular zone being more strongly stained and the peri-epidermal zone more weakly stained (Fig. 5(a,b,e)). This staining gradient appears to be linked to the density of fibres in the different zones (see above). These staining patterns indicate that neutral polysaccharides, probably in the form of cellulose fibrils, are present in both the cuticular and fibrous layers. However, they seem to be more abundant in the latter where they are associated with sulphated proteoglycans and basic proteins. This is consistent with the composition of the tunic fibrils in *H. papillosa* which consist of a cellulosic core surrounded by a sheath made up of acid mucopolysaccharides and proteins [19]. The different types of granulocytes stain for both proteins and neutral carbohydrates (Figs. 2(c,d) and 5(b,c)). Those present in the median zone of the fibrous layer (presumably dense-granular amoebocytes) also stain with the NBT redox cycling method indicative of redox active groups, but the absence of staining with Arnow's method indicates that these groups are neither catechol (DOPA) nor pyrogallol (TOPA) groups.

Raman spectroscopy measurements confirmed the histochemistry results. Although the spectra acquired from the cuticular layer were quite noisy due to a very strong fluorescence background even with near-infrared laser (785 nm), clear peaks in the region between 1000 and 1700 cm^{-1} could be observed (Fig. 5(h)). The peak at 1004 cm^{-1} is typical of the amino acid phenylalanine in proteins and the amide I protein band was observed centred at 1663 cm^{-1} [35]. Thus, these data further support the proteinaceous composition of the cuticular layer. In comparison, Raman spectra acquired from the fibrous layer were significantly less fluorescent and showed an entirely different set of peaks (Fig. 5(h)). In particular, several sharp peaks are prominent in spectra from this region, which are characteristic for the presence of cellulose, including peaks at 380 cm^{-1}, 1096 cm^{-1} and 1129 cm^{-1} [35,36].

FTIR spectroscopy was performed to further investigate the composition of the tunic. The FTIR spectra of both the cuticular and fibrous layers are shown in Fig. 5(i). The peaks around 3000 cm^{-1} are attributed to the C–H aliphatic stretching and the overlapped bands near 3300 cm^{-1} are generally for OH stretching (at 3336 cm^{-1}) and amide A band (at 3302 cm^{-1}) [37,38]. The strong bands at 1649 and 1541 cm^{-1} are the amide I and II bands, respectively – indicative of proteins [38]. In contrast, in the region around 1100 cm^{-1}, four sharp peaks can be observed at wavenumbers around 1036, 1061, 1115, and 1163 cm^{-1} (Fig. 5(i)), which are characteristic peaks for cellulose [38]. Notably, very similar spectral features were observed from the tunic of the ascidian tunicate *Ciona intestinalis* [39] suggesting a common composition across

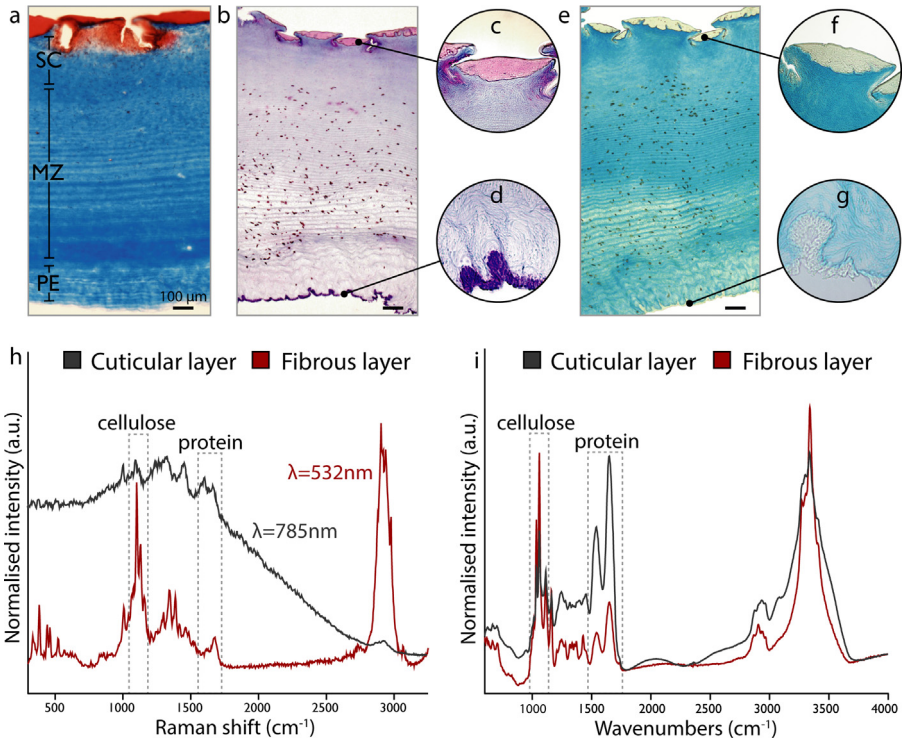

Fig. 5. Histochemical and vibrational spectroscopic investigation of tunic composition in *Halocynthia roretzi*. Transverse sections through the tunic stained with Astra blue and counterstained with acid fuschin (a), stained with PAS and counterstained with luxol blue (b–d), and stained with alcian blue at pH 1 (e–g). (c,f) Details of a cuticular scale on top of the subcuticular zone. (d,g) Details of the epidermis and the peri-epidermal zone. Raman (h) and FTIR (i) spectroscopic measurements performed on the two tunic layers. Abbreviations: MZ, median zone; PE, peri-epidermal zone; SC, subcuticular zone. (For interpretation of the references to colour in this figure legend, the reader is referred to the web version of this article.)

different orders of Ascidiacea. The spectra of the tunic cuticular and fibrous layers present similar peaks indicating that both layers contain proteins and cellulose. However, the relative peak intensities differ significantly between layers, indicating a higher proportion of proteins in the cuticular layer and a higher relative amount of cellulose in the fibrous layer. Along these lines, a closer look at the Raman spectra reveals weak cellulose peaks in the cuticle spectra and weak protein peaks in the fibrous layer. The spectroscopic data showing co-localization of proteins and cellulose in varying ratios in the cuticle and fibrous regions are consistent with the TEM and AFM observations, the histochemical staining, as well as tunic compositions reported for other species [13–15].

The strong fluorescent background observed with Raman spectroscopy at the level of the cuticular layer prompted us to investigate the auto-fluorescence of the tunic in epifluorescence microscopy. A specific auto-fluorescence of the cuticular layer was observed with all the filter sets tested, but it was the strongest with the blue emission filter (Fig. 6(a)). A strong blue auto-fluorescence (with a maximum at 400 nm) is characteristic of biomaterials containing dityrosine cross-links (Fig. 6(b)), such as the cuticles and elastic ligaments of insects, the cell walls of some species of fungi, the cuticles of some species of nematodes, and some invertebrate cross-linked egg membranes [40–42]. This type of crosslinking presumably stabilizes all these naturally occurring, protein-based structural materials. To confirm the presence of dityrosine in the cuticular layer of *H. roretzi*, fresh cuticle samples were acid hydrolysed and their amino acid composition was analysed and compared to a dityrosine standard (Fig. 6(c)). The cuticular material contains about 3 mol% of dityrosine residues based on amino acid analysis (Table 1). Dityrosine cross-links may have important implications for mechanical properties. In resilin, the insect ligament protein, they allow long-range deformability and a nearly perfect elastic recovery [43]. In caddisfly larvae silk fibres, the dityrosine-crosslinked outer sheath provides a restoring force to the self-recovering silk fibres strained past their yield point [44].

Table 1
Amino acid composition of the tunic cuticular layer in *Halocynthia*.

	Halocynthia roretzi[a]	*Halocynthia papillosa*[b]
Asx	11.7	13.4
Thr	6.3	6.1
Ser	7.2	9.5
Glx	7.6	10.5
Gly	9.5	12.8
Ala	7.2	5.3
Cys	4.3	6.3
Val	6.4	5.5
Met	1.9	ND
Ile	4.6	4.2
Leu	5.3	3.9
Tyr	4.3	0.3
Phe	4.3	4.6
Dityr	3.2	ND
His	2.9	0.6
Lys	6.8	8.4
Arg	5.3	4.7
Pro	1.2	3.8
Total	100	99.9

ND, not determined.
[a] Present study.
[b] Lübbering-Sommer et al. [22].

Areas of differential contrast were observed on the backscattered electron (BSE) images of tunic transverse sections (Fig. 7(b)). The brightness in such images is proportional to the atomic number, Z [45], and thus, the lighter colouration of the cuticular scale in Fig. 7(b) is indicative of a larger concentration of heavy elements. The elemental distribution was analysed by energy

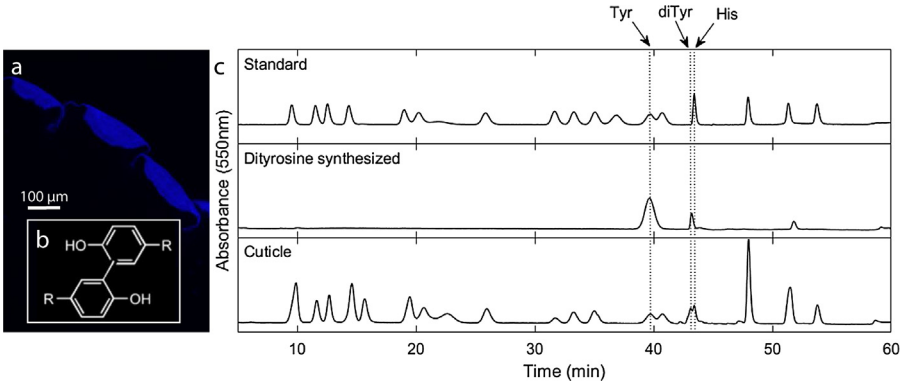

Fig. 6. Highlighting of dityrosine cross-links in the tunic cuticular layer of *Halocynthia roretzi*. (a) Epifluorescence microscopy of an unstained tunic sections. The strong blue autofluorescence of the cuticular layer is indicative of dityrosine cross-links (b). (c) Amino acid chromatograms from an amino acid mix standard, a dityrosine standard prepared as described in the Material and Methods section, and an acid hydrolysis of fresh cuticular material. (For interpretation of the references to colour in this figure legend, the reader is referred to the web version of this article.)

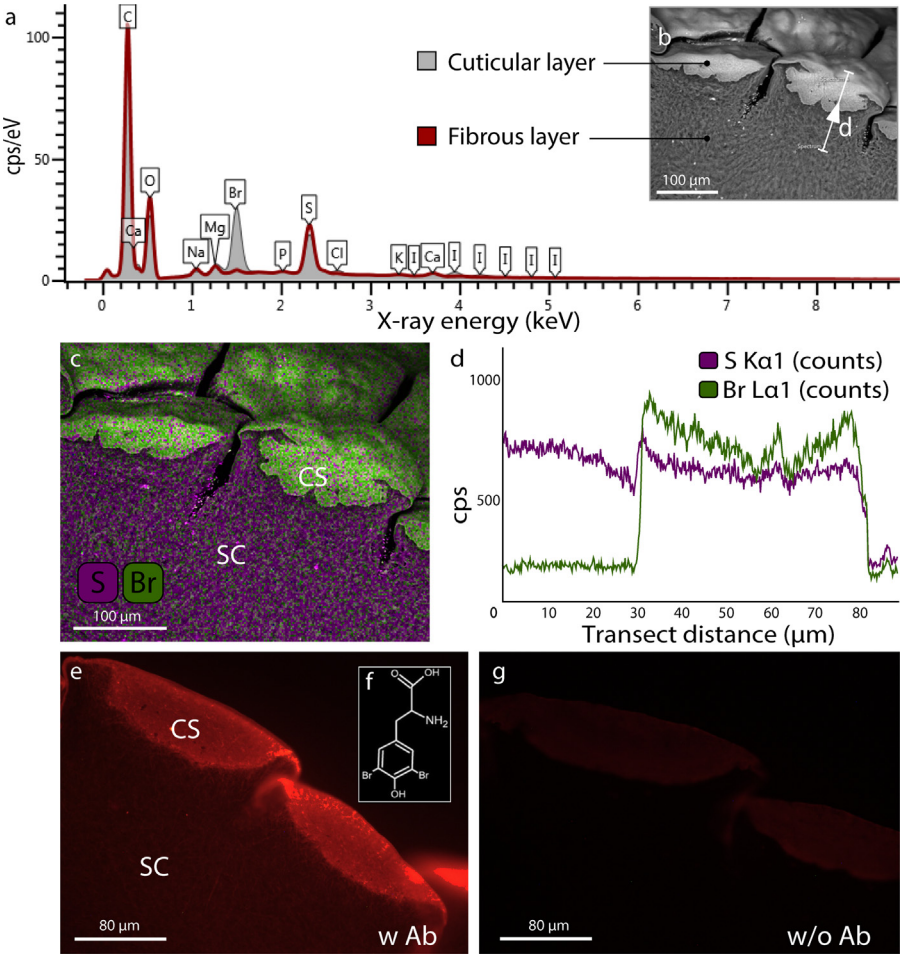

Fig. 7. Composition of the tunic cuticular layer in *Halocynthia roretzi*. (a) Representative EDS spectra from the cuticular layer (grey-filled peaks) and from the subcuticular zone of the fibrous layer (open curve), as indicated in (b). (b) BSE SEM image of a section through the outer part of the tunic. (**c**) Same SEM image showing EDS spatial maps for bromine and sulphur. (d) Distribution of these two elements along the EDS line scan represented by the white line in (b). The scan was from bottom to top. (e–g) Immunofluorescence labelling (in red) using anti-bromotyrosine (f) antibodies. Transverse section through the outer part of the tunic showing a specific labelling of the cuticular layer (e). This labelling disappears in the control reaction when antibodies are omitted, except for the residual auto-fluorescence (g). Abbreviations: cps, counts per second; keV, kiloelectron volts. (For interpretation of the references to colour in this figure legend, the reader is referred to the web version of this article.)

dispersive X-ray spectroscopy (EDS). Fig. 7(a) shows two such spectra taken at the level of the cuticular scale and of the subcuticular zone, as indicated in Fig. 7(b). The spectra show strong signals from C, O, Br and S, and small amounts of Ca, Na, P, Cl and I (Fig. 7(a)). The Br and I signals are exclusively present in the spectrum taken from the cuticular layer. These observations were confirmed by the mapping of some elements over the entire sample in which the Br distribution map matches perfectly the cuticular scales (Fig. 7(c)) and by a line scan across the subcuticular zone-cuticular layer transition (Fig. 7(d)). It is noteworthy that, in

H. papillosa, Lübbering-Sommer et al. [22] reported a similarly specific signal in the cuticular spines, but assigned as aluminium. As Br Lα is sometimes misidentified by some software systems as Al Kα in the EDS spectra of bromine-containing compounds [46], Br-rich scales could be a characteristic feature of the cuticular layer in the genus *Halocynthia*. Another element of interest is sulphur. Indeed, although histochemistry demonstrated that sulphated proteoglycans are exclusively present in the fibrous layer, sulphur concentration did not vary significantly along the transect line crossing the tunic (Fig. 7(d)). This suggest that sulphur in the cuticular layer has a different origin and could derive from cysteine-rich proteins (Table 1; see also [22]).

The presence of bromine is common at the surface of some biological materials. It has been described in the outer cuticle of the jaws of marine polychaetes [47] and of the tip of crustacean appendages such as the claws of crabs and woodlice [48–50]. Using different techniques, such as mass spectrometry or X-ray absorption spectroscopy, the authors investigating these biological materials reported that Br is bound to proteins in the form of brominated amino acids such as tyrosine [47,48]. To check whether the bromine we detected in the tunic of *H. roretzi* is also bound to proteins in the cuticular layer, we used a monoclonal anti-halotyrosine antibody specifically recognizing mono- and dibromotyrosine (Fig. 7(f)) and, to a lesser degree, chlorotyrosine [51]. Within the tunic, immunoreactivity was restricted to the cuticular layer, and the scales in particular were strongly immunolabelled (Fig. 7(e)). When the primary antibody was omitted, only a weak autofluorescence was observed (Fig. 7(g)). The specific immunolabelling confirms that Br in the cuticular scales is in the form of mono- or dibromotyrosine presumably within the protein fraction of the cuticular material. In polychaete jaws and crab claws, it has been proposed that the function of bromine could be to increase fracture resistance of the outer cuticle and render it less susceptible to chemical and enzymatic attack [47,48]. Interestingly, both dityrosines and halogenated tyrosines can be obtained from peroxidase activity [44,47]. Peroxidase uses H_2O_2 as a substrate to catalyse a one-electron oxidation of Tyr to form a tyrosine free radical [52]. Tyrosine free radicals can combine with one another and with halogens to form dityrosine and bromotyrosine, respectively.

3.3. Structure of the tunic

Hierarchical structure of biomolecular building blocks is a common feature of most composite biological materials, including insect cuticle, wood and bone [53]. In order to further investigate the multiscale structure of the tunic, we employed polarized light microscopy (PLM), SEM and wide-angle X-ray diffraction (WAXD). PLM uses orthogonally oriented polarizers to visualize birefringence and thus, molecular orientation in materials. Using a quarter wavelength phase retardation plate, we investigated the birefringence of thin sections of the tunic (Fig. 8). The orange coloration reveals that the biomolecules (presumably cellulose based on staining) within longitudinal sections of the fibrous layer are oriented primarily parallel to the long axis, while regions exhibiting the same pink colour as the background are presumably oriented out of the plane of the image. This is reminiscent of the helicoidal arrangement of cellulose, which is commonly observed in different biological materials comprised of cellulose, chitin and collagen [54,55]. Indeed, SEM imaging of the median zone of the fibrous layer of *H. roretzi* on sections cut obliquely appear to show a transition in cellulose orientation that varies in a helicoidal fashion (Fig. 8(d,e)), as it was suggested for *H. papillosa* [15] and *H. aurantium* [56]. PLM suggests a periodicity varying between 5 and 15 µm for this helicoidal pattern, which corresponds perfectly to the spacing measured between the layers of the median zone of the fibrous layer on histological sections (see 3.1. above). The

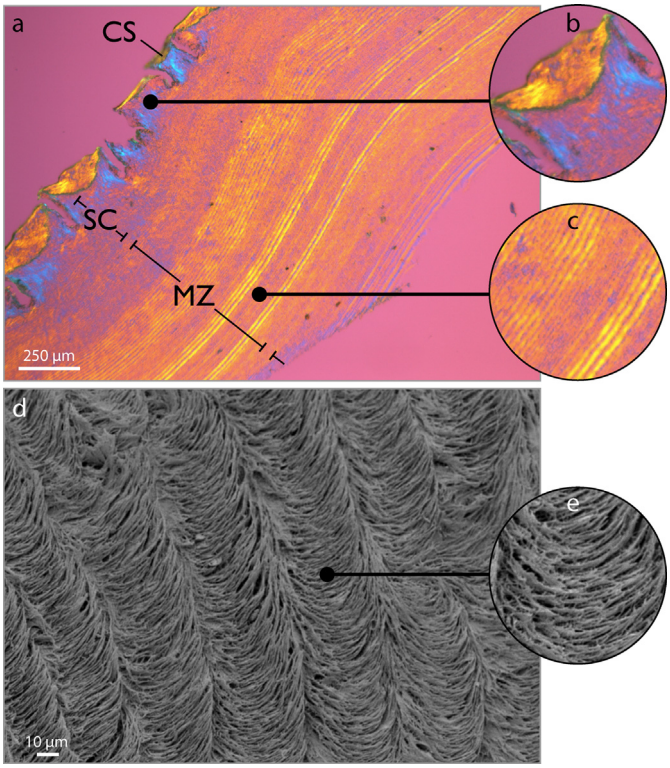

Fig. 8. Fibre arrangement in the tunic of *Halocynthia roretzi*. (a,c) Polarized light microscopy images with lambda (λ) compensator of a longitudinal section through the tunic. General view of the tunic (a) and details of the cuticular (b) and fibrous (c) layers. (d,e) Scanning electron microscopy images of an oblique section of the tunic median zone. Abbreviations: CS, cuticular scale; MZ, median zone of the fibrous layer; SC, subcuticular zone of the fibrous layer.

largest periodicity observed in SEM (i.e., 30 to 50 µm) is due to the very oblique sections through the tunic used to visualize the helicoidal arrangement of the fibres. Notably, in the PLM images, the orientation of cellulose appears to change significantly in the regions immediately adjacent to the cuticular layer, which exhibit blue coloration (i.e. the cellulose fibrils are primarily oriented perpendicular to those in the bulk of the matrix).

X-ray diffraction can provide insights both into the presence and crystallinity of cellulose in materials, as well as its preferential orientation within materials. Previously, X-ray diffractometry was performed on *H. roretzi* tunic material [57]; however, orientational data of these reflections was not reported. Additionally, WAXD measurements were made on uniaxially oriented films cast from cellulose extracted from *H. papillosa* [29]. However, as far as we know the orientation of the cellulose within the tunic of *Halocynthia* spp. was not previously investigated with WAXD. Here, WAXD measurements made within the fibrous layer of longitudinal sections of the tunic indicate the presence of cellulose based on the appearance of reflections, which correspond to the 200 and 110/1–10 reflections of crystalline cellulose, respectively [57]. Notably, in measurements made in the subcuticular (SC) zone, the reflections appear ring-like (Fig. 9(b)), whereas in the median zone (MZ), they appear as distinct and well-defined equatorial reflections (Fig. 9(c)). These different profiles reveal a stark difference in the degree of cellulose orientation in the respective regions. To investigate this trend further, we plotted the azimuthal distribution of the 200 reflection at each position made along a continuous line scan from the cuticular layer through the subcuticular and median zones (Fig. 9(a) and (d)), further revealing that the cellulose fibrils closest to the cuticle are less oriented based on the broader distribution of the peaks, while cellulose throughout the fibrous region

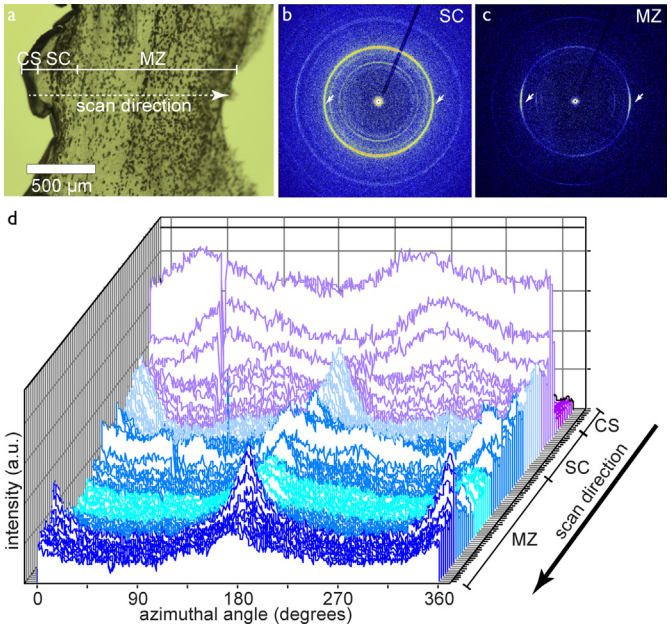

Fig. 9. WAXD analysis of transverse sections through the tunic of *Halocynthia roretzi*. (a) Light microscope image of a transverse tunic section used for WAXD analysis, showing scanning direction and zones. (b,c) Representative WAXD patterns collected from (b) the subcuticular zone (SC) and (c) median zone (MZ). White arrows indicate the 200 reflection in panels (b) and (c). (e) Azimuthal intensity plots of the 200 reflection at each point along a line scan moving from the cuticular scale (CS) through the subcuticular layer and the median zone.

is well-oriented in a nearly perpendicular direction with a much narrower azimuthal distribution. In several patterns, a second set of peaks appear at different azimuthal angles, possibly indicating a second orientation co-existing with the first; however, at this time, it is challenging to explain the origin of these peaks within the 3-dimensional structure of the tunic. These general trends were found to be consistent between 5 different sections acquired from several individual organisms, indicating them to be characteristic features of the tunic. Notably, we did not observe a helicoidal transition in the cellulose orientation as suggested by the PLM and SEM data; however, this is likely due to the fact that our beam size of 10 µm is in the range of periodicity observed with the other methods (~5–15 µm), thus, averaging the orientation. While these data provide important new insights into the hierarchical structure of the tunic, further investigation is required to more precisely determine the 3-dimensional organization of the cellulose fibrils at smaller length scales.

4. Conclusion

Based on our combined compositional and structural studies of the tunic of *H. roretzi*, a clearer picture of this biological material is emerging. Compositionally, the tunic is a composite comprised of nanoscale cellulose microfibrils in a protein matrix; however, the relative ratios of the cellulose/proteins vary significantly between the outer cuticular layer and the inner fibrous layer. Structurally, we observed a large degree of variation in the orientation of the cellulose between the cuticular and fibrous layers, and even within the fibrous region, such that the cellulose appears loosely organized near the surface of the tunic and well-ordered deeper within. Indeed, closer to the animal, the cellulose appears to be organized in layers in which the orientation of the cellulose crystals varies in a helicoidal manner. This has been observed in numerous other biological materials comprised of cellulose, but also of chitin and even collagen [54,58]. The functional relevance of this variation in structural organization is unclear at this point, but in other organisms, similar helicoidal organization of fibrous biomolecules plays a role in improved toughness by hindering and deflecting the propagation of crack paths through the material [59]. Whether the cellulose organization in the tunic of *H. roretzi* plays a similar role remains to be seen, but this would be consistent with the proposed function of the tunic as a tough protecting layer. The outer cuticular layer comprised of sclerotized protein reinforced with cellulose nanofibrils may accordingly play a protective role. This protein matrix is brominated and cross-linked with dityrosine bonds. Biomaterials presenting a similar composition usually form tough flexible coatings [42,47,48]. In *H. roretzi*, the cuticular layer could therefore provide abrasion resistance in marine intertidal zones where sand and other debris are kicked up into the water column by crashing waves. However, both of these proposed roles await further microscale mechanical characterization of the tunic. Regardless, the tunic of the sea pineapple provides an interesting new role model for the design of cellulosic composites.

Authors contributions

PF, MJH and DSH designed the research; HBK and DSH collected the organisms, fixed tunic samples and conducted amino acid analyses; PF, GS, JD and DS made LM and SEM observations and performed EDS analyses; JD and DS made TEM observations; TCN and PL conducted AFM analyses; PF performed the immunolabelling; GS, NH and MJH conducted the Raman and FTIR spectroscopic analyses, as well as the PLM and WAXD measurements and analysed the data; PF, GS and MJH wrote the first draft of the manuscript; JD and MJH prepared the figures; and all co-authors revised and approved the final manuscript.

Declaration of Competing Interest

The authors declare no conflict of interest, financial or otherwise.

Acknowledgements

PF, MJH and DSH acknowledge support of a KONNECT Bilateral European-Korean Seed Grant (NRF-2015K1A3A1A59074243 (KR); FNRS ERA-NET n° R.50.16.16.F (BE); and BMBF 01DR16006 (DE)). MJH acknowledges additional support from the Max Planck Society. We thank S. Siegel and C. Li at the mySpot beamline (BESSY, Adlershof-Berlin, Germany) for scientific and technical support and M. Eder for helpful discussion. JD, PF and PhL are respectively Postdoctoral Researcher, Research Director and Senior Research Associate of the Fund for Scientific Research (F.R.S.-FNRS) of Belgium. DSH acknowledges additional support from National Research Foundation of Korea (2016M3D3A1A01913258)

References

[1] E.E. Ruppert, R.S. Fox, R.D. Barnes, in: Invertebrate Zoology: A Functional Evolutionary Approach, Saunders College Pub, Fort Worth, 2003, p. 1008p.
[2] B.J. Swalla, A.B. Smith, Deciphering deuterostome phylogeny: molecular, morphological and palaeontological perspectives, Phil. Trans. R. Soc. Lond. B 363 (2008) 1557–1568.
[3] C. Monniot, F. Monniot, P. Laboute, Coral Reef Ascidians of New Caledonia, ORSTOM Edition, 1991.
[4] P. Burighel, R.A. Cloney, Urochordata: ascidiacea, in: F.W. Harrison, E.E. Ruppert (Eds.), in Microscopic Anatomy of Invertebrate, Hemichordata, Chaetognatha, and the Invertebrate Chordates, vol. 15, Wiley-Liss, 1997, pp. 221–347.
[5] P. Burighel, R.A. Cloney, F.W. Harrison, E.E. Ruppert (Eds.), Wiley-Liss, 1997.
[6] P.S. Belton, S.F. Tanner, N. Cartier, H. Chanzy, High-resolution solid-state ^{13}C nuclear magnetic resonance spectroscopy of tunicin, an animal cellulose, Macromolecules 22 (1989) 1615–1617.
[7] A.G. Matthysse, K. Deschet, M. Williams, M. Marry, A.R. White, W.C. Smith, A functional cellulose synthase from ascidian epidermis, Proc. Natl Acad. Sci. U.S.A. 101 (2003) 986–991.

[8] K. Nakashima, L. Yamada, Y. Satou, J. Azuma, N. Satoh, The evolutionary origin of animal cellulose synthase, Dev. Genes Evol. 214 (2004) 81–88.
[9] J. Inoue, K. Nakashima, N. Satoh, ORTHOSCOPE analysis reveals the presence of the cellulose synthase gene in all tunicate genomes but not in other animal genomes, Genes 10 (2019) 294.
[10] E. Hirose, Ascidian tunic cells: morphology and functional diversity of free cells outside the epidermis, Invertebrate Biol. 128 (2009) 83–96.
[11] E. Hirose, K. Nakayama, T. Yanagida, A. Nawata, S.-I. Kitamura, Measurement of tunic hardness in an edible ascidian, *Halocynthia roretzi*, with remarks on soft tunic syndrome, Zool. Sci. 35 (2018) 548–552.
[12] M.J. Smith, The blood cells and tunic of the ascidian *Halocynthia aurantium* (Pallas). I. Hematology, tunic morphology, and partition of cells between blood and tunic, Biol. Bull. 138 (1970) 354–378 a.
[13] M.J. Smith, The blood cells and tunic of the ascidian *Halocynthia aurantium* (Pallas). II. Histochemistry of the blood cells and tunic, Biol. Bull. 138 (1970) 379–388 b.
[14] J. Stievenart, Recherches sur la morphologie et étude histochimique de la tunique d'*Halocynthia papillosa* Gun. (Ascidie stolidobranche), Ann. Soc. R. Zool. Belg. 601 (1971) 25–56.
[15] Y. Van Daele, G. Goffinet, Composition chimique et organisation de la tunique de deux ascidies : *phallusia mammillata* et *Halocynthia papillosa*, Ann. Soc. R. Zool. Belg. 117 (1987) 181–199.
[16] E. Hirose, S.-I. Ohtake, K. Azumi, Morphological characterization of the tunic in the edible ascidian *Halocynthia roretzi* (Drasche), with remarks on 'soft tunic syndrome' in aquaculture, J. Fish Dis. 32 (2009) 433–445.
[17] S.-I. Kitamura, S.-I. Ohtake, J.-Y. Song, S.-J. Jung, M.-J. Oh, B.-D. Choi, K. Azumi, E. Hirose, Tunic morphology and viral surveillance in diseased Korean ascidians: soft tunic syndrome in the edible ascidian, *Halocynthia roretzi* (Drasche), in aquaculture, J. Fish Dis. 33 (2010) 153–160.
[18] A. Schmidt-Rhaesa, in: The Evolution of Organ Systems, Oxford University Press, Oxford, 2007, p. 385p.
[19] Y. Van Daele, J.-F. Revol, F. Gaill, G. Goffinet, Characterization and supramolecular architecture of the cellulose-protein fibrils in the tunic of the sea peach (*Halocynthia papillosa*, Ascidiacea, Urochordata), Biol. Cell 76 (1992) 87–96.
[20] B. Lübbering-Sommer, P. Compère, G. Goffinet, Cytochemical investigations on tunic morphogenesis in the sea peach *Halocynthia papillosa* (Tunicata, Ascidiacea) 1: demonstration of polysaccharides, Tissue Cell 28 (1996) 621–630.
[21] S. Kimura, T. Itoh, Cellulose synthesizing terminal complexes in the ascidians, Cellulose 11 (2004) 377–383.
[22] B. Lübbering-Sommer, P. Compère, G. Goffinet, Cytochemical investigations on tunic morphogenesis in the sea peach *Halocynthia papillosa* (Tunicata, Ascidiacea) 2: demonstration of proteins, Tissue Cell 28 (1996) 651–661.
[23] E. Kontturi, P. Laaksonen, M.B. Linder, Nonappa, A.H. Gröschel, O.J. Rojas, O. Ikkala, Advanced materials through assembly of nanocelluloses, Adv. Mater. 30 (2018) 1703779.
[24] N. Grishkewich, N. Mohammed, J. Tang, K.C. Tam, Recent advances in the application of cellulose nanocrystals, Curr. Opin. Colloid Interface Sci. 29 (2017) 32–45.
[25] Y. Zhao, J. Li, Excellent chemical and material cellulose from tunicates: diversity in cellulose production yield and chemical and morphological structures from different tunicate species, Cellulose 21 (2014) 3427–3441.
[26] G. Lambert, R.C. Karney, W.Y. Rhee, M.R. Carman, Wild and cultured edible tunicates: a review, Manag. Biol. Invasions 7 (2016) 59–66.
[27] S.H. Song, J.E. Kim, E.K. Koh, J.E. Sung, H.A. Lee, W.B. Yun, J.T. Hong, D.Y. Hwang, Selenium-loaded cellulose film derived from *Styela clava* tunic accelerates the healing process of cutaneous wounds in streptozotocin-induced diabetic Sprague–Dawley rats, J. Dermatol. Treat. 29 (2018) 606–616.
[28] H.-J. Hong, H. Yu, M. Park, H.S. Jeong, Recovery of platinum from waste effluent using polyethyleneimine-modified nanocelluloses: effects of the cellulose source and type, Carbohydr. Polym. 210 (2019) 167–174.
[29] W. Helbert, Y. Nishiyama, T. Okano, J. Sugiyama, Molecular imaging of *Halocynthia papillosa* cellulose, J. Struct. Biol. 124 (1998) 42–45.
[30] M. Gabe, in: Techniques Histologiques, Masson, Paris, 1968, p. 1113p.
[31] M. Paz, R. Flückinger, A. Boak, H.M. Kagan, P.M. Gallop, Specific detection of quinoproteins by redox-cycling staining, J. Biol. Chem. 266 (1991) 689–692.
[32] L.E. Arnow, Colorimetric determination of components of 3,4-dihydroxyphenyl-L-alanine/tyrosine mixtures, J. Biol. Chem. 118 (1937) 531–537.
[33] R. Amado, R. Aeschbach, H. Neukom, Dityrosine: in vitro production and characterization, Meth. Enzymol. 107 (1984) 377–388.
[34] Y. Van Daele, G. Goffinet, J. Godeaux, Structure des fibres cellulose-protéiques de la tunique d'*Halocynthia papillosa* Gün. (Ascidiacea, Stolidobranchiata), Bull. Soc. R. Liège 57 (1988) 59–68.
[35] Z. Movasaghi, S. Rehman, I.U. Rehman, Raman spectroscopy of biological tissues, Appl. Spectrosc. Rev. 42 (2007) 493–541.
[36] U.P. Agarwal, Raman imaging to investigate ultrastructure and composition of plant cell walls: distribution of lignin and cellulose in black spruce wood (*Picea mariana*), Planta 224 (5) (2006) 1141–1153.
[37] J. Kong, S. Yu, Fourier transform infrared spectroscopic analysis of protein secondary structures, Acta Biochim. Biophys. Sin. 39 (2007) 549–559.
[38] Z. Movasaghi, S. Rehman, I.U. Rehman, Fourier transform infrared (FTIR) spectroscopy of biological tissues, Appl. Spectrosc. Rev. 43 (2008) 134–179.
[39] K. Nakashima, J. Sugiyama, N. Satoh, A spectroscopic assessment of cellulose and the molecular mechanisms of cellulose biosynthesis in the ascidian *Ciona intestinalis*, Mar. Genom. 1 (2008) 9–14.
[40] D.A. Malencik, S.R. Anderson, Dityrosine as a product of oxidative stress and fluorescent probe, Amino Acids 25 (2003) 233–247.
[41] J. Michels, E. Appel, S.N. Gorb, Resilin – the pliant protein. Pp 89-136 in E. Cohen, B. Moussian (Eds), Extracellular Composite Matrices in Arthropods, Springer, Switzerland, 2016.
[42] B.P. Partlow, M.B. Applegate, F.G. Omenetto, D.L. Kaplan, Di-tyrosine crosslinking in designing biomaterials, ACS Biomater. Sci. Eng. 2 (2016) 2108–2121.
[43] J. Michels, E. Appel, S.N. Gorb, Functional diversity of resilin in Arthropoda, Beilstein J. Nanotechnol. 7 (2016) 1241–1259.
[44] C.-S. Wang, N.N. Ashton, R.B. Weiss, R.J. Stewart, Peroxinectin catalyzed dityrosine crosslinking in the adhesive underwater silk of a casemaker caddisfly larvae, *Hysperophylax occidentalis*, Insect Biochem. Mol. Biol. 54 (2014) 69–79.
[45] J.J. Bozzola, L.D. Russell, in: Electron Microscopy – Principles and Techniques for Biologists, Jones and Bartlett Publishers, Boston, 1992, p. 542p.
[46] D.E. Newbury, Mistakes encountered during automatic peak identification of minor and trace constituents in electron-excited energy dispersive X-ray microanalysis, Scanning 31 (2009) 91–101.
[47] H. Birkedal, R.K. Khan, N. Slack, C. Broomell, H.C. Lichtenegger, F. Zok, G.D. Stucky, J.H. Waite, Halogenated Veneers: protein cross-linking and halogenation in the jaws of *Nereis*, a marine polychaete worm, ChemBioChem 7 (2006) 1392–1399.
[48] R.M.S. Schofield, J.C. Niedbala, M.H. Nesson, Y. Tao, J.E. Shokes, R.A. Scott, M.J. Latimer, Br-rich tips of calcified crab claws are less hard but more fracture resistant: a comparison of mineralized and heavy-element biological materials, J. Struct. Biol. 166 (2009) 272–287.
[49] M. Katsikini, Detailed spectroscopic study of the role of Br and Sr in coloured parts of the *Callinectes sapidus* crab claw, J. Struct. Biol. 195 (2016) 1–10.
[50] M. Vittori, V. Srot, K. Zagar, B. Bussmann, P.A. van Aken, M. Ceh, J. Štrus, Axially aligned organic fibers and amorphous calcium phosphate form the claws of a terrestrial isopod (Crustacea), J. Struct. Biol. 195 (2016) 227–237.
[51] H. Jin, T.S. Hallstrand, D.S. Daly, M.M. Matzke, P. Nair, D.J. Bigelow, J.G. Pounds, R.C. Zangar, A halotyrosine antibody that detects increased protein modifications in asthma patients, J. Immunol. Methods 403 (2014) 17–25.
[52] H. Eickhoff, G. Jung, A. Rieker, Oxidative phenol coupling – tyrosine dimers and libraries containing tyrosyl peptide dimers, Tetrahedron 57 (2001) 353–364.
[53] P. Fratzl, R. Weinkamer, Nature's hierarchical materials, Prog. Mater. Sci. 52 (2007) 1263–1334.
[54] M.-M. Giraud-Guille, Plywood structures in nature, Curr. Opin. Solid State Mater. Sci. 3 (1998) 221–227.
[55] S.E. Naleway, M.M. Porter, J. McKittrick, M.A. Meyers, Structural design elements in biological materials: application to bioinspiration, Adv. Mater. 27 (2015) 5455–5476.
[56] S. Kimura, T. Itoh, Biogenesis and function of cellulose in the tunicates, in: R.M. Brown Jr., I.M. Saxena (Eds.), in Cellulose: Molecular and Structural Biology, Springer, 2007, pp. 217–236.
[57] S. Kimura, K. Nakayama, M. Wada, U.-J. Kim, K. Azumi, T. Ojima, A. Nozawa, S.-I. Kitamura, E. Hirose, Cellulose is not degraded in the tunic of the edible ascidian *Halocynthia roretzi* contracting soft tunic syndrome, Dis. Aquat. Org. 116 (2015) 143–148.
[58] M.-M. Giraud-Guille, G. Mosser, E. Belamie, Liquid crystallinity in collagen systems in vitro and in vivo, Curr. Opin. Colloid Interface Sci. 13 (2008) 303–313.
[59] Z. Song, Y. Ni, S. Cai, Fracture modes and hybrid toughening mechanisms in oscillated/twisted plywood structure, Acta Biomater. 91 (2019) 284–293.